High pretilt four-domain twisted nematic liquid crystal display by microrubbing : process, characterization and optical simulation

High pretilt four-domain twisted nematic liquid crystal display by microrubbing: Process, characterization, and optical simulation

Soney Varghese,[a] Gregory P. Crawford, and Cees W. M. Bastiaansen[b]
Department of Polymer Technology, Faculty of Chemistry and Chemical Engineering, Eindhoven University of Technology, P.O. Box 513, NL-5600 MB Eindhoven, The Netherlands

Dick K. G. de Boer and Dirk J. Broer
Philips Research Laboratories, Professor Holstlaan 4, NL-5656 AA Eindhoven, The Netherlands and Department of Polymer Technology, Faculty of Chemistry and Chemical Engineering, Eindhoven University of Technology, P.O. Box 513 NL-5600 MB Eindhoven, The Netherlands

(Received 9 August 2004; accepted 6 December 2004; published online 8 February 2005)

A microrubbing (μ-rubbing) technique was utilized to create four-domain alignment in a liquid crystal display sample. A small metallic sphere under sufficient load was used to directly rub a homeotropic polyimide alignment layer to create a large surface pretilt angle. We demonstrate a 47-μm linewidth and a variable pretilt angle with respect to the substrate plane for different loads. The homeotropic polyimide surface was μ rubbed in such a way that neighboring alignment regions are rubbed in opposite directions. liquid crystal cells were constructed with two μ-rubbed substrates where the rubbing directions are orthogonal to each other. With this cell configuration we obtained four domains consisting of two left-handed and two right-handed twisted nematic subpixels. We report on the electro-optic performance properties, viewing angle characteristics, the relationship between pretilt angle versus load, and thermal aging study of the four-domain liquid crystal cell. The optical simulations of the liquid crystal director orientation, viewing angle characteristics, and the contrast ratio of the four domains are also presented. The experimental results are in agreement with the simulation results. © *2005 American Institute of Physics*. [DOI: 10.1063/1.1854203]

I. INTRODUCTION

In the liquid crystal display (LCD) industry much attention is focused on improving the viewing angle of the display, especially for large area displays such as those poised to enter the television market. The viewing angle problem in conventional twisted nematic LCD arises from the fact that the midplane liquid crystal (LC) director angle (optic axis) is uniformly oriented in one direction creating a highly anisotropic viewing dependence. Due to the inherent birefringence of LC material, different viewing directions give varying degrees of birefringence resulting in optical transmission behavior being strongly dependent on the viewing direction.[1] Furthermore the electro-optic switching characteristics of uniformly aligned twisted nematic (TN) displays are strongly dependent on the viewing angle, a serious drawback for stable gray scale performance. A wide viewing angle for all levels of gray is a prerequisite for full color, high-resolution displays.[2]

There are many approaches to overcome the poor viewing angle performance in LCDs, which involve compensation films integrated on the outside of the display,[3,4] inside the display cell modifications involving multidomain alignment,[5–8] vertical alignment,[9–11] and alternative modes of operation such as in-plane switching (IPS).[12–14] Retardation film approaches, especially those involving tilted negative birefringence, improve the viewing angle but they are relatively complex and add significantly to the display costs. Multidomain alignment requires a number of lithographic steps,[5–8] which is unattractive for manufacturing; therefore, researchers have focused on accomplishing the same goal using patterned photo alignment,[15] oblique evaporation of silicon oxide,[16,17] and writing with atomic force microscopy (AFM) tip.[18,19]

Here we present a comprehensive study on fabricating multidomain twisted nematic cells by utilizing a microrubbing (μ-rubbing) process. The μ-rubbing process has also recently been used for fabricating liquid crystal gratings.[20] In this study, the viewing angle characteristics, contrast ratio, electro-optical characteristics, and director orientations are demonstrated by means of experiments and numerical simulations. This is a comprehensive study that leverages our earlier letters paper.[21]

II. EXPERIMENT

A. Materials

Polyimide precursor for the orientation layer AL75114 was procured from JSR electronics. Indium tin oxide (ITO) coated glass (25×25 mm^2) was obtained from Merck Ltd., Darmstadt, Germany. The ITO coated glass substrates were thoroughly washed with a soap solution and de-ionized water followed by an ethanol rinse and then dried. The polyimide precursor was spin coated (5 s at 1000 rpm followed by 40 s at 5000 rpm) on the ITO side of the glass substrate. It is then preheated to 100 °C for 10 min and imidized at 180 °C under vacuum for 90 min to get a transparent film with a thickness of ~100 nm. The liquid crystal E7, a mixture consisting

[a]Electronic mail: s.varghese@tue.nl
[b]Electronic mail: c.w.m.bastiaansen@tue.nl

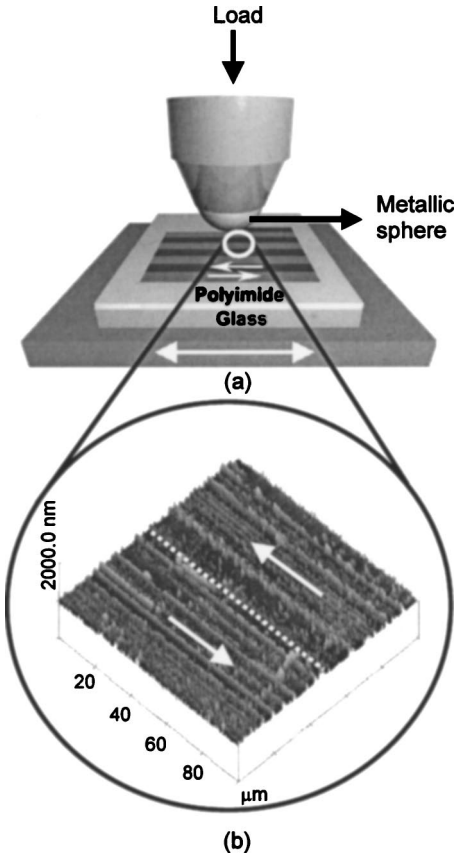

FIG. 1. Illustration of experimental setup for the μ-rubbing process, the arrows show the direction of μ rubbing (a). Atomic force microscopy image of the μ-rubbed surface where homeotropic polyimide having two lines with opposite rubbing direction are adjacent to each other (b).

of 50.6% K15 (4-pentyl-4′-cyanobiphenyl), 25.2% K21 (4-heptyl-4′-cyanobiphenyl), 17.8% M24 (4-octyloxy-4′-cyanobiphenyl), and 6.4% T15 (4-pentyl-4′-cyanoterphenyl), was obtained from Merck Ltd., Darmstadt, Germany.

B. The μ-rubbing process

The μ-rubbing technique utilizes a metallic sphere (1 mm diameter) to physically rub the alignment layer. We utilize a polyimide alignment layer that induces homeotropic anchoring of the liquid crystal in the unrubbed state. The metallic sphere is in direct contact with the alignment layer as it traverses across the substrate creating micrometer-sized rubbed lines at a velocity of 10 mm/min under specified load at room temperature. The μ-rubbing apparatus at the instrument level consists of a metallic sphere secured to a rigid post, which can move in both the X and Y directions with high precision. A load is exerted on the top of this post during the μ-rubbing process. The polyimide substrate is firmly secured to a translational stage. We utilized our μ-rubbing technique to create multidomain pixels by rubbing the surface in such a way that neighboring alignment regions are rubbed in opposite directions, as schematically depicted in Fig. 1(a).

C. Cell construction

liquid crystal cells were constructed with two μ-rubbed substrates placing the rubbing directions of the bottom plate and the top plate orthogonal to each other and securing them with UV curable glue (Norland UV sealant 91) along the edges. The cell gap was controlled with 5 μm spacers. The cells were filled with the liquid crystal E7 by capillary action at 80 °C, which is ~20 °C above the nematic-isotropic transition temperature of liquid crystals.

D. Characterization

Surface morphology of the μ-rubbed polyimide layer was investigated by AFM, Nanoscope Dimension 5000 AFM with a Nanoscope III controller (Digital Instruments, Santa Barbara, CA) with a scan rate of 1 Hz. Cell gap measurements were carried out using Shimadzu UV-3102 PC UV-Vis-NIR scanning spectrophotometer. Electro-optical measurements were performed on a DMS 703 display measuring system (autronic-Melchers Gmbh). ac square wave was used to drive the display cells (1 kHz). The alignment of liquid crystals was studied using a Zeiss LM Axioplan polarized light microscope. The pretilt angle was measured directly using an autronic-Melchers TBA 107 instrument that uses the crystal rotation method.[22] Viewing angle characteristics were measured using an Eldim conoscope up to an azimuthal angle of 60° under various voltages using a wave form generator.

III. MODELING METHODS

There are different numerical methods available for the calculation of director profiles, viewing angle characteristics, and electro-optical behavior of the LCDs. Simulation methods for director profiles are derived from the Oseen–Frank free-energy equation for the electric and elastic energies of the liquid crystal given by the following expression:[23]

$$F = \frac{1}{2}\int_v [k_{11}(\vec{\nabla}\cdot\hat{n})^2 + k_{22}(\hat{n}\cdot\vec{\nabla}\times\hat{n})^2 + k_{33}(\hat{n}\times\vec{\nabla}\times\hat{n})^2 - \varepsilon_0\Delta\varepsilon(\vec{E}\cdot\hat{n})^2]dv,$$

where k_{11}, k_{22}, and k_{33} are the splay, twist, and bend elastic constants, respectively, $\Delta\varepsilon$ is the dielectric anisotropy, $\hat{n}$ is the nematic director, $\vec{E}$ is the applied electric field, and ε_0 is the permittivity of free space. Vector representation methods are usually used in most simulation algorithms. From this expression, the director profile can be derived using the appropriate boundary conditions. There are two ways to solve the resulting equations in the numerical calculations, the finite difference method (FDM) and the finite element method (FEM). The FEM is generally used because of its flexibility. The two-dimensional simulations of the director profiles were made with the 2dimMOS software package[24,25] using a vector representation and the FEM with a mesh of triangular elements.

For the calculation of the optical transmission of a LCD cell the extended Jones method was used, which takes into account single reflection at each surface but neglects mul-

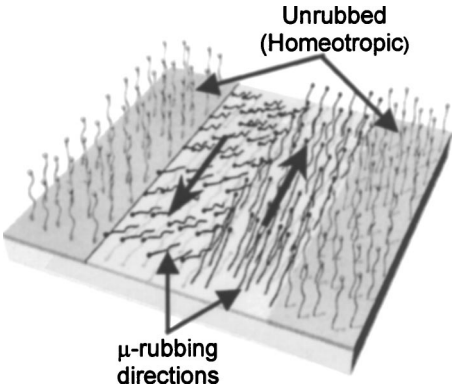

FIG. 2. A schematic illustration of a surface rich in aliphatic moieties and its deformation during the μ-rubbing process.

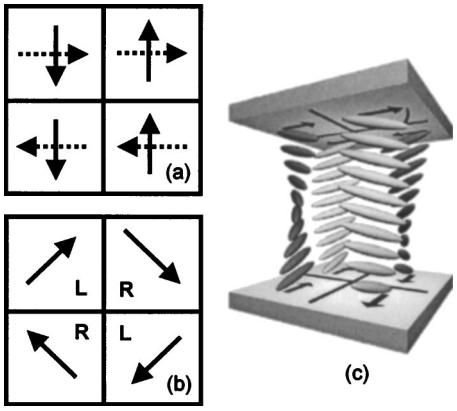

FIG. 3. Orientation of liquid crystal directors in four different domains. The solid and dotted arrows indicate the rubbing direction of the top and bottom substrates (a). The direction of the midplane directors in the four domains, L and R indicate left and right twist of the liquid crystal (b). Four domains schematically showing the opposite twist sense in each subpixel (c).

tiple reflections and their interference. This method provides a systematic way to analyze the propagation of monochromatic plane waves in a layered birefringent medium.

IV. RESULTS AND DISCUSSION

In order to perform the μ-rubbing process, a metallic sphere comes in direct contact with the homeotropic layer, as shown in Fig. 1(a). The metallic sphere has an average surface roughness of 8.0 ± 0.5 nm measured with AFM. After this process is complete, we find that the orientation of the liquid crystal that comes in contact with the surface is planar with a large surface pretilt angle. The linewidth (pixel size) can be controlled by changing the applied load or by changing the metallic sphere diameter. In the first set of experiments we employed a constant 150 g load. Figure 1(b) shows the AFM image of the μ-rubbed surface. The single linewidth is found to be ~ 47 μm with an average surface roughness of 40 ± 2 nm, as determined by AFM. As can be observed from our AFM measurements in Fig. 1(b), μ-rubbing does generate grooves on homeotropic polyimide with a width of several micrometers. However, we do not believe that these relatively wide grooves are responsible for the observed alignment. Alternatively we propose the following mechanism.

Polyimides that are known to induce homeotropic anchoring are either modified by the addition of long chain aliphatics or are functionalized with long chain aliphatic molecules. When aliphatic chains pack on a substrate parallel to the substrate normal (highly aligned, compact assembly of aliphatic chains), they are known to induce homeotropic alignment of liquid crystal molecules coming in contact with them. We conjecture that the μ-rubbing process unidirectionally aligns the aliphatic chains at a specific angle, as schematically shown in Fig. 2. This mechanism leads to a dramatic change in the anchoring direction for the liquid crystal molecules interacting with the surface.

Figure 3(a) shows the rubbing directions on the top and bottom substrates. The orthogonal alignment of the liquid crystal molecules anchored to the surface and the tilt angle impose the twist, its direction (handedness), and the average tilt over the cross section of the layer. Figure 3(b) shows the midplane tilt direction of the various domains in the center of the cell. A three-dimensional (3D) rendition of a multidomain pixel is depicted in Fig. 3(c). Due to the difference in the rubbing direction in this multidomain configuration, we have two left-handed and two right-handed subpixels, in which the midplane directors are oriented in four corners of the subpixels. Since we engineered our samples to have a 47 μm pixel size, we were unable to measure the pretilt angle directly in a given subpixel using the crystal rotation method.[22] Therefore, we constructed single domain cells, using unidirectional parallel rubbing of the substrates, so that we could perform the pretilt angle measurements. Antiparallel rubbed cells were constructed with a cell gap of 18 μm and filled with the liquid crystal E7, the pretilt was measured to be $9.8° \pm 0.5$. To study the variation of the pretilt with applied load we have fabricated LC cells having a TN area made under different loads on the same substrate in order to have a constant cell gap (5 μm). To make the TN area bigger for the pretilt measurement we have made parallel lines in the same direction touching each other to get an area of 2 mm^2. The pretilt observed for the 150 g load from this TN cell was $7.2° \pm 0.5$, which is 2.6° less measured from the antiparallel cell. It can be attributed to the difference in cell construction and the difference in cell gap. Figure 4 depicts the variation of the pretilt with applied load; here we can observe that the pretilt decreases with load. The aliphatic moieties that induce homeotropic boundary conditions are

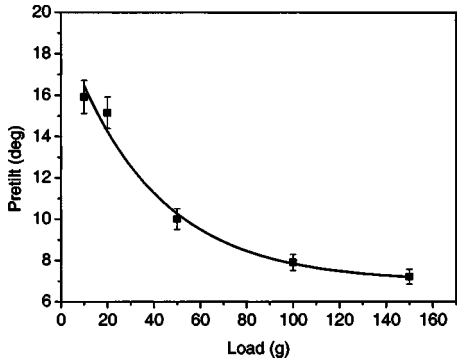

FIG. 4. The relationship between surface pretilt angles and applied load measured using crystal rotation method.

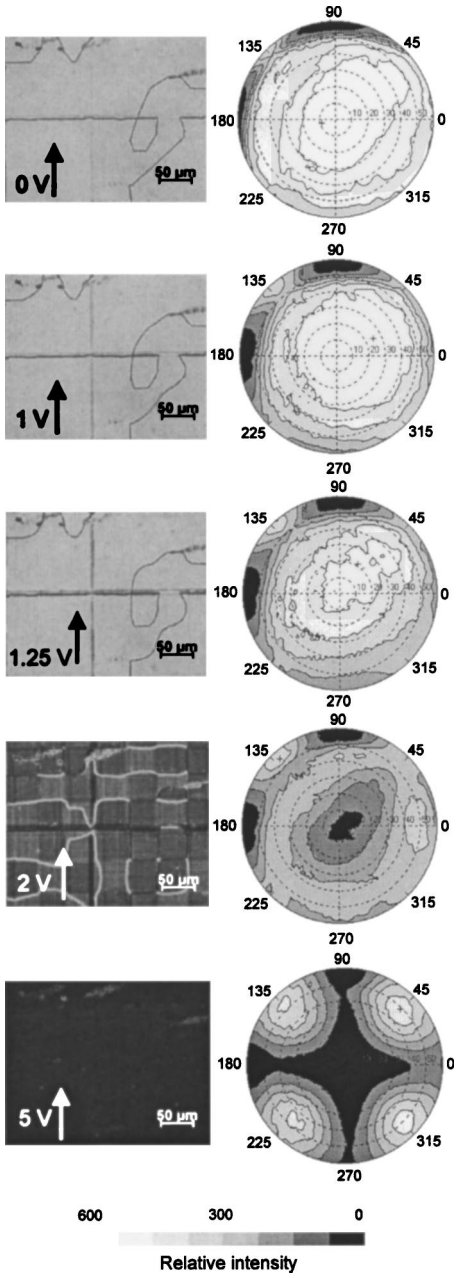

FIG. 5. Optical microscopy images of a four-domain twisted nematic cell created by the μ-rubbing process situated between crossed polarizers and subjected to an applied voltage 0–5 V. The contrast as a function of viewing angle of the four-domain TN cell under the same voltage is also shown. The dark line in the image at 2 V is due to a small lateral gap between two μ-rubbed lines.

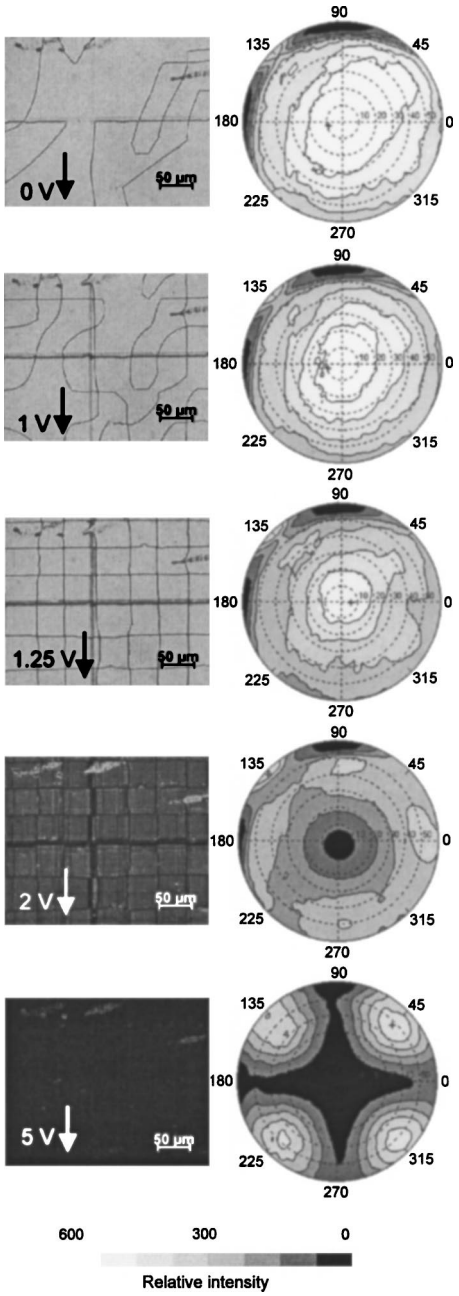

FIG. 6. Optical microscope photograph of a four-domain twisted nematic cell created by the μ-rubbing process situated between crossed polarizers and subjected to an applied voltage 5–0 V. The contrast as a function of viewing angle of the four-domain TN cell under the same voltage is also shown. The dark line in the image at 2 V is due to a small lateral gap between two μ-rubbed lines.

deformed with load, this deformation determines the pretilt angle of the LC molecules. Being able to control the surface pretilt angle with this simple method would be useful for many applications.

Figure 5 presents the polarizing optical microscope photographs of four-domain TN cell and its corresponding viewing angle characteristics measured with an Eldim conoscope as a function of applied voltage 0 V$\rightarrow$5 V (increasing voltage), and in Fig. 6 decreasing voltage (5 V$\rightarrow$0 V). The two different bias tilt directions on each substrate define the appropriate sense of the four subtwisted pixel configurations. On the macroscopic scale, the optical anisotropies of the differently aligned midplane tilt angles of the four subhelices compensate each other, as depicted schematically in Figs. 3(b) and 3(c). The angular dependence of a four-domain display is significantly reduced as compared to conventional single domain TN LCDs.[17] When the sample is switched from 0 to 5 V in small increments we observe the formation of unstable disclination lines at 2 V and it transforms into a perfectly dark state at 5 V (homeotropic). The four-domain structure becomes more stable for voltages greater than 2 V. When we slowly reduce the voltage from 5 to 0 V, we could see the clear disclination lines indicating a stable four-domain configuration over a large voltage range. The larger

dark lines in Figs. 5 and 6 at 2 V are due to a small lateral gap between two μ-rubbed lines (splay configuration with one surface having homeotropic alignment and other surface having parallel alignment). The occurrence of this is due to the spatial resolution of our μ-rubbing apparatus. The viewing angle measurements of the four-domain TN cell at five different voltages are also presented in Figs. 5 and 6. Upon lowering the voltage to 1.25 V, we observe the symmetric nature of the isointensity curves, inherent of the multidomain twisted nematic configuration.[15,16]

The twisted states in our samples are completely determined by the pretilt angle; therefore, a large surface pretilt angle is required to offset the energy cost of the generation of twist disclinations. In order to ascertain the stability of our four-domain samples in zero field, one needs to compare the free-energy cost associated with forming disclination lines and the wrong handedness subpixel orientations that cost splay energy. In our polarizing microscope photographs unstable disclination lines are still visible at 2 V for increasing voltages (Fig. 5), whereas for decreasing voltages (Fig. 6), the disclination lines are stable down to 1.25 V.

Using a simple model proposed by Chen *et al.*[16] based on the tilt angle θ, subpixel dimensions $L \times L$, and the cell gap d, from the known elastic and defect properties of nematic liquid crystals, the stability condition can be expressed by the following equation: $\theta^2 \geqslant \pi d/L$. Using $L \sim 50$ μm and $d \sim 5$ μm, the predicted minimum pretilt angle, $\theta_{\min}$, to stabilize the structure is $\theta_{\min} \sim 30°$. Since our cells have only a pretilt of $\sim 10°$, our zero-field structures do not have four-domain stable structures. Although this model is simple, it is consistent with our findings and the work presented in the literature.[16,17] Therefore, in our sample at zero voltage and at low-voltage states where the disclination lines disappear or become unstable, the four domains essentially transform into a two-domain reverse tilt sample. It is possible to stabilize the four-domain structure using a voltage initialization process and driving the sample with bilevel voltages. This scheme can completely lock-in the motion of disclination lines.[17] We essentially demonstrated this phenomena by reducing the voltage after domains were formed at high voltage.

Figure 7 shows the enlarged optical micrograph of the stable four-domain structures in which the midplane directors are oriented in four corners indicated by the arrows. The two different bias tilt directions on each substrate define the appropriate sense of the four twisted subpixel configurations. Figure 8(a) shows the comparison of transmission/voltage characteristics of our four-domain sample (pretilt, $9.8° \pm 0.5$) to a conventional TN cell (with $2.65° \pm 0.5$ pretilt angle). Very little difference exists between the four-domain and the conventional cell. There are two notable features that standout in Fig. 8(a). First, the steepness of the transmission-voltage curve of the four-domain is "softened" due to the large pretilt. Second, the brightness is lower in the four-domain sample due to the disclination lines. Both of these effects are expected as a consequence of four-domain alignment. We further calculated the transmission-voltage curve

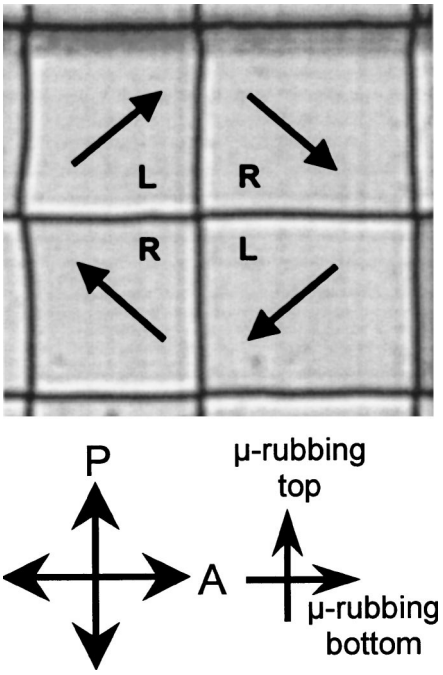

FIG. 7. Optical microscopy image of the four-domain structure which is stable above 1 V, the direction of the midplane directors are indicated by the arrows.

using the extended Jones matrix method for our large pretilt sample in Fig. 8(b). The experimental and optical simulation results are in good agreement.

Figure 9 shows the two-dimensional (2D) director patterns (vertical cross sections) simulated with the 2DIMMOS program. This figure depicts the vertical cross sections of the cell having two subpixels. The gray rods represent the direc-

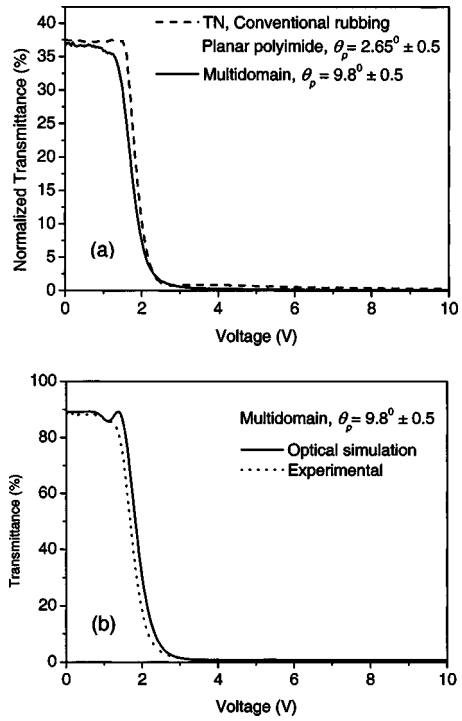

FIG. 8. Transmission-voltage curves of a conventional TN cell compared to a μ-rubbed multidomain TN cell (a). Experimental and simulated transmission-voltage curves of a multidomain TN display (b).

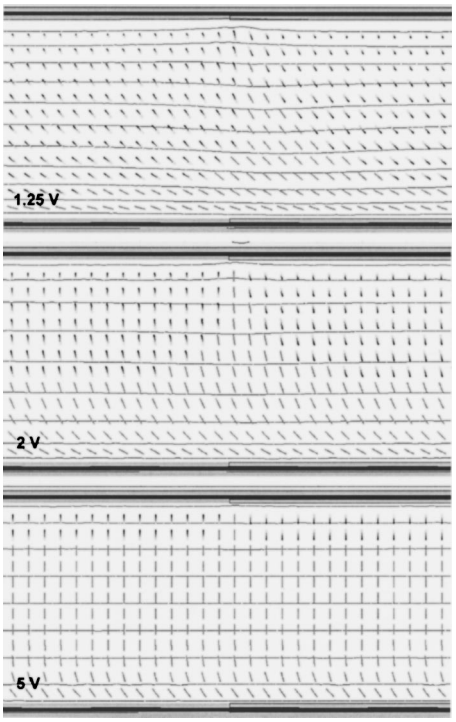

FIG. 9. Results of the 2dimMOS calculation for the director orientation of four-domain cell at (a) 1.25 V, (b) 2 V, and (c) 5 V. Top left pretilt=10° azimuthal=90°, top right pretilt=10° azimuthal=270°, and bottom pretilt =10° azimuthal=180°. The gray rods represent the directors, where the light end indicates a forward direction and the dark ends indicate a backward direction with respect to the plane of drawing.

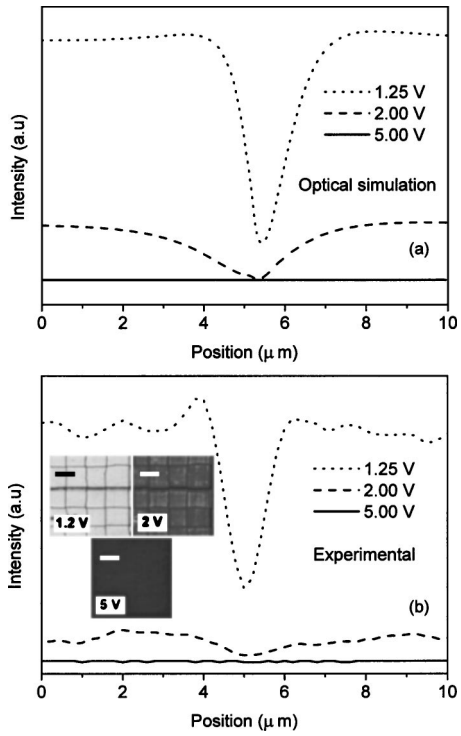

FIG. 10. Comparison of the calculated (a) and experimental (b) intensity profile over the disclination lines at different voltages. Optical microscopy images of the disclination lines at the same voltages are also shown, the line at the top left shows the scanned area.

tors, where the light end indicates a forward direction and the dark ends indicate a backward direction with respect to the plane of drawing. In this calculation we selected a cross section of a pair of μ-rubbed patterns on the top substrate and a single μ-rubbed pattern on the bottom substrate, which are orthogonal to each other. The left half of the top substrate is having a pretilt of 10° (μ-rubbed area) with an azimuthal angle of 90° and the right half is having the same pretilt with an azimuthal angle of 270°. The bottom substrate also possesses the same pretilt with an azimuthal angle of 180°. From the simulation study we observe the orientation of directors in applied field and the formation of disclination lines. In Fig. 9 the directors in the two domains are inclined in opposite directions. At 1.25 V this results in a disclination line in which the director rotates over 180°, giving rise to dark regions in the transmission, as shown in Fig. 10(a), which are comparable with our experimental observations in Fig. 6. At higher voltage the disclination lines disappear to give a perfectly dark state (homeotropic state). Table I lists the liquid crystal parameters used in the optical simulation.

Figure 10(b) shows the line scans of the optical microscopy image at 1.25, 2, and 5 V. For the line scans a straight line was drawn over the image across the disclination lines and the intensity versus position was plotted. The experimental and optical simulation results are in good agreement. At 1.25 V the disclination lines appear due to the difference in the orientation of the directors in each subpixel. A slight asymmetry is seen in the curve. The intensity versus position changes more steeply on the left side of the disclination since there the twist helps to align the directors in the plane of drawing, parallel to one of the polarizer directions.

Figure 11 depicts the optical simulation of the viewing angle characteristics of the four-domain TN cell, calculated using the extended Jones method. At 1.25 V we could observe the symmetric nature of isointensity curves, typical for multidomains. These results are comparable with our experimental results shown in Fig. 6. The theoretical and experimental calculations of isocontrast measurements (ratio of brightness at 1.25 and at 5 V) of the four-domain cell are shown in Fig. 12. We could observe the improvement in contrast uniformity and symmetry, especially at higher viewing angles. In the direction perpendicular or parallel to one of the polarizers the contrast ratio is 40:1 at angles $> \pm 50°$. At 45° to the polarizers a contrast ratio of 10:1 is possible up to

TABLE I. Parameters of TN cell used in the optical simulations. (The parameters of LC E7 are used.)

Dielectric anisotropy	$\varepsilon_{\parallel}$	19.0
(20 °C, 1 kHz)	$\varepsilon_{\perp}$	5.2
	$\Delta\varepsilon$	+13.8
Elastic constants (20 °C)	k_{11}	11.1pN
	k_{33}	17.1pN
	k_{33}/k_{11}	1.54
Optical anisotropy	Δn	0.2253
(20 °C, 589 nm)	n_e	1.7464
	n_o	1.5211
Cell gap (μm)	d	5.0
Pretilt angle	θ	9.8°±0.5
Twist angle	ϕ	90°

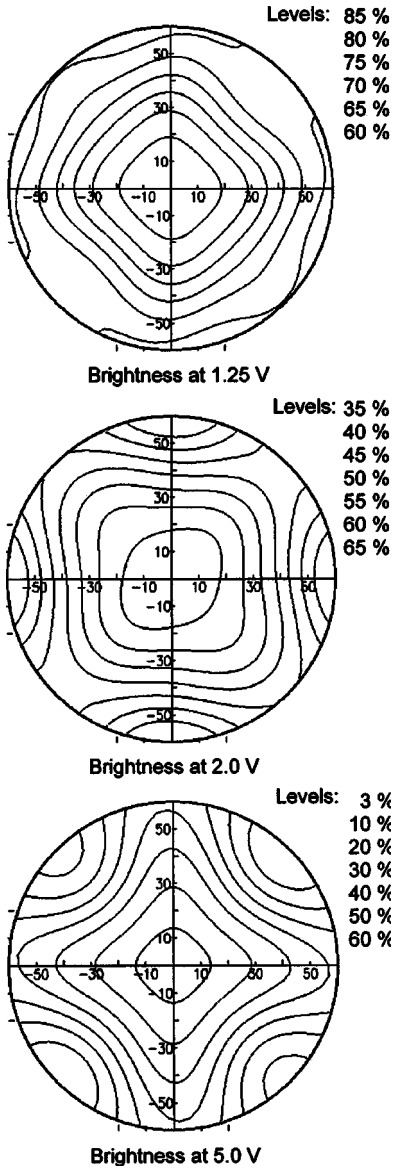

FIG. 11. The optical simulation results of the brightness vs viewing angle of the four-domain at 1.25, 2, and 5 V.

±30°. The optical calculation using the extended Jones method is in good agreement with the experimental observation. It is possible to further improve the viewing angle of our four-domain configuration by integrating with negative birefringence compensation film on the sample. Chen *et al.*[16] have shown through simulations that a nearly symmetric viewing angle and inversion free zones exist for polar angles $\leqslant 50°$ when a negative birefringence film is used with the four-domain alignment. This approach can also be used in our samples. The four-domain approach will undoubtedly result in reduced brightness due to the dark disclination lines, as shown in Fig. 6.

Because the controlled four-domain formation in our samples is supposed to be the result of a realignment of packed aliphatic moieties at the polyimide surface, we were concern with possible relaxation of these units and the corresponding loss of orientation and favorable electro-optic properties. Therefore, we performed the following thermal aging study where the sample was heated to 100 °C and kept

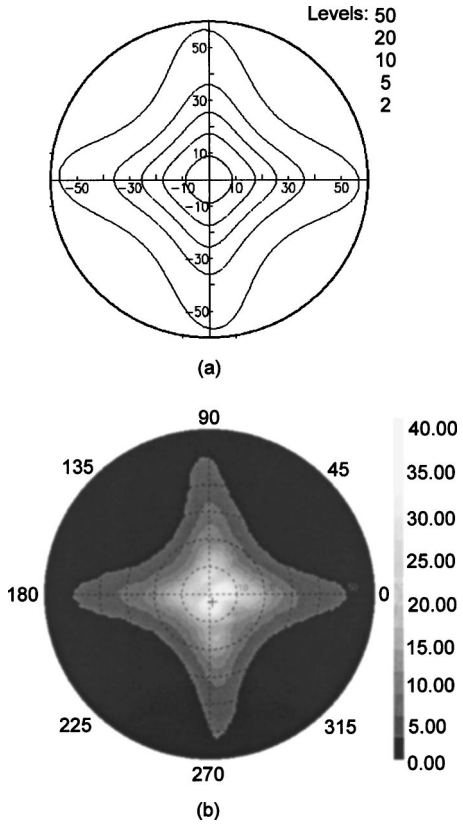

FIG. 12. The theoretical calculations (a) and experimental results (b) of the contrast ratio vs viewing angle of the four-domain liquid crystal-cell.

isothermally for 15 min and then cooled to room temperature at 20 °C. The sample was then allowed to stabilize at 20 °C for 15 min before taking the transmission-voltage data. We repeated this heating protocol five times, as shown in Fig. 13. The transmission-voltage curve in Fig. 13 remains relatively unchanged with only a minor shift of $\Delta V \sim 0.1V$ (at 50% transmission). This brought us to the conclusion that the alignment as imposed by μ rubbing of a homeotropic polyimide is sufficiently stable and robust to serve in applications such as high-end displays.

V. CONCLUSIONS

In conclusion, we have fabricated multidomain twisted nematic configuration using a reverse μ-rubbing process. The μ-rubbing process can be used to generate a multido-

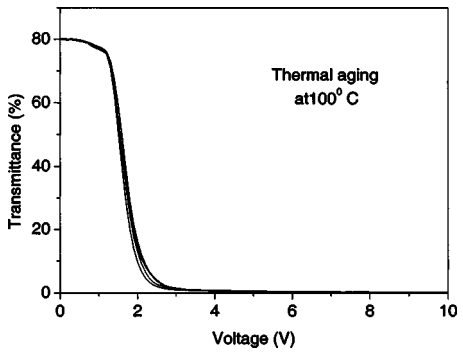

FIG. 13. Transmission-voltage curve of the four-domain cell after heat aging at 100 °C under different time intervals (15 min).

main configuration with a high surface pretilt angle, in our case ~10° for a 150 g load with a 1 mm metallic sphere, with the possibility of higher pretilt angle for lower loads. Our four-domain samples are not stable in the zero voltage state since our surface pretilt angle is below that needed for a stable structure for a given pixel dimensions and cell gap. It only becomes stable at high voltages. Our optical simulation results agree well with the experimental observations. The 2D modeling of the director pattern and the viewing angle measurements are useful for a better understanding of their electro-optical properties. Our μ-rubbing technique is straightforward, flexible, economical, and simple to execute. We believe this technique can be scaled up and used in the production of large area displays.

ACKNOWLEDGMENTS

Funding of this project was provided by the Netherlands University Federation for International Collaboration (Nuffic). The authors thank Dr. Sunil K. Narayanankutty, Cochin University of Science and Technology, India, Dr. Hugo Cornelissen, Mark Hage, Rogier Cortie, Philips Research, and Chris van Heesch, Eindhoven University of Technology for their support.

[1] S. W. Depp and W. E. Howard, Sci. Am. **266**, 40 (1993).
[2] S. Musa, Sci. Am. **277**, 87 (1997).
[3] N. Yamagishi, H. Watanabe, and K. Yokoyama, J. Soc. Inf. Disp. **1989**, 316.
[4] Y. Yamagnchi, T. Miyashita, and T. Uchida, J. Soc. Inf. Disp. **1993**, 277.
[5] J. Li, E. S. Lee, H. Vithana, and P. J. Bos, Jpn. J. Appl. Phys., Part 2 **35**, L1446 (1996).
[6] H. Yoshida, T. Seino, and Y. Koike, Jpn. J. Appl. Phys., Part 2 **36**, L1449 (1997).
[7] K. H. Yang, Jpn. J. Appl. Phys., Part 2 **31**, L1603 (1992).
[8] H. Vithana, D. Johnson, P. Bos, R. Herke, Y. K. Fung, and S. Jamal, Jpn. J. Appl. Phys., Part 1 **35**, 2222 (1996).
[9] D. S. Seo and J. Y. Hwang, Jpn. J. Appl. Phys., Part 2 **39**, L914 (2000).
[10] K. Ohmuro, S. Kataoka, T. Saski, and Y. Koike, J. Soc. Inf. Disp. **1997**, 845.
[11] D. S. Seo and J. Y. Hwang, Jpn. J. Appl. Phys., Part 2 **38**, L1432 (1999).
[12] R. A. Soref, J. Appl. Phys. **45**, 5466 (1974).
[13] M. Oh-e and K. Kondo, Appl. Phys. Lett. **67**, 3895 (1995).
[14] M. Oh-e and K. Kondo, Appl. Phys. Lett. **69**, 623 (1996).
[15] M. Schadt, H. Seiberle, and A. Schuster, Nature (London) **381**, 212 (1996).
[16] J. Chen, P. J. Bos, D. L. Johnson, D. R. Bryant, J. Li, S. H. Jamal, and J. R. Kelly, J. Appl. Phys. **80**, 1985 (1996).
[17] J. Chen, P. J. Bos, D. R. Bryant, D. L. Johnson, S. H. Jamal, and J. R. Kelly, Appl. Phys. Lett. **67**, 1990 (1995).
[18] G. P. Sinha, C. Rosenblatt, and L. V. Mirantsev, Phys. Rev. E **65**, 041718 (2002).
[19] B. Wen, M. P. Mahajan, and C. Rosenblatt, Appl. Phys. Lett. **76**, 1240 (2000).
[20] M. Honma and T. Nose, Jpn. J. Appl. Phys., Part 1 **42**, 6992 (2003).
[21] S. Varghese, G. P. Crawford, C. W. M. Bastiaansen, D. K. G. de Boer, and D. J. Broer, Appl. Phys. Lett. **85**, 230 (2004).
[22] B. L. V. Horn and H. H. Winter, Appl. Opt. **40**, 2089 (2001).
[23] P. G. de Gennes and J. Prost, *The Physics of Liquid Crystals* (Oxford University Press, New York, 1994).
[24] M. E. Becker, H. Wohler, M. Kamm, and J. Kreis, J. Soc. Inf. Disp. **1996**, 596.
[25] 2dimMOS, www.autronic-melchers.com